



Lawrence Berkeley Laboratory

UNIVERSITY OF CALIFORNIA

RECEIVED
LAWRENCE
BERKELEY LABORATORY

MAY 6 1981

LIBRARY AND
DOCUMENTS SECTION

Submitted to Nuclear Physics

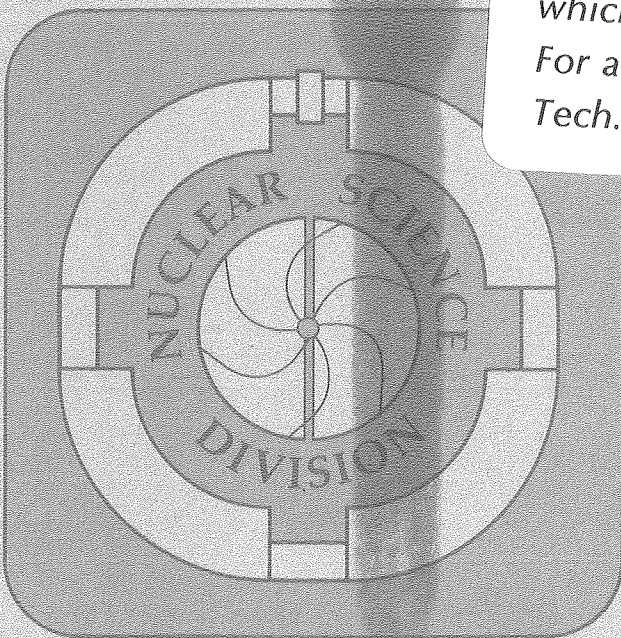
ANGULAR MOMENTUM TRANSFER AND PARTITION IN THE
DEEP-INELASTIC REACTION: $664 \text{ MeV } ^{84}\text{Kr} + \text{natAg}$

L.G. Sobotka, C.C. Hsu, G.J. Wozniak, D.J. Morrissey,
and L.G. Moretto

April 1981

TWO-WEEK LOAN COPY

*This is a Library Circulating Copy
which may be borrowed for two weeks.
For a personal retention copy, call
Tech. Info. Division, Ext. 6782.*



LBL-11840
c. 2

DISCLAIMER

This document was prepared as an account of work sponsored by the United States Government. While this document is believed to contain correct information, neither the United States Government nor any agency thereof, nor the Regents of the University of California, nor any of their employees, makes any warranty, express or implied, or assumes any legal responsibility for the accuracy, completeness, or usefulness of any information, apparatus, product, or process disclosed, or represents that its use would not infringe privately owned rights. Reference herein to any specific commercial product, process, or service by its trade name, trademark, manufacturer, or otherwise, does not necessarily constitute or imply its endorsement, recommendation, or favoring by the United States Government or any agency thereof, or the Regents of the University of California. The views and opinions of authors expressed herein do not necessarily state or reflect those of the United States Government or any agency thereof or the Regents of the University of California.

Angular Momentum Transfer and Partition in the Deep-Inelastic Reaction:
664 MeV $^{84}\text{Kr} + \text{natAg}^*$

L.G. Sobotka, C.C. Hsu**, G.J. Wozniak,
D.J. Morrissey, and L.G. Moretto

Nuclear Science Division
Lawrence Berkeley Laboratory
University of California
Berkeley, CA 94720

Abstract: In- and out-of-plane angular distributions have been measured for sequential alpha decay from target-like fragments produced in fully relaxed heavy-ion collisions. At angles equal to or larger than the target-recoil direction, the α -particle energy spectra are evaporation-like and the in-plane angular distributions are consistent with isotropy in the rest frame of the target recoil. The out-of-plane distributions exhibit an anisotropy of approximately two. Fragment spins were extracted from these distributions as a function of mass asymmetry. These spins are in agreement with those obtained from a simultaneous gamma-ray multiplicity measurement. Both the fragment kinetic energies and intrinsic spins are consistent with rigid rotation of an intermediate complex consisting of two substantially deformed spheroids in near proximity.

E

NUCLEAR REACTIONS $^{107,109}\text{Ag}(^{84}\text{Kr},x)$, $E = 664$ MeV; measured $\sigma(E,\theta,Z)$ for α , M_γ ; deduced fragment spins.

* This work was supported by the Director, Office of Energy Research, Division of Nuclear Physics of the Office of High Energy and Nuclear Physics of the U.S. Department of Energy under Contract W-7405-ENG-48.

**Permanent address: Institute of Atomic Energy, Beijing, China.

I. Introduction

Studies of deep inelastic (DI) heavy ion collisions have led to the concept of a short-lived, rotating dinuclear complex^{1,2} which, after dissipating a variable amount of the entrance channel kinetic energy, separates into projectile-like and target-like fragments. Measurements of the energy loss are sensitive to both the radial and tangential components of the frictional force. On the other hand, measurements of the angular momentum imparted to the final fragments specifically probe the tangential component of the frictional force.³ This spin transfer process has been investigated by determining either the sum of the spins of the two fragments, or the spin of an individual fragment. The sum of the spins has been extracted from γ -ray multiplicity data³⁻⁹, M_γ , whereas the spin of an individual fragment has been commonly extracted from the out-of-plane angular distributions of sequential fission fragments.¹⁰⁻¹³ The determination of both the individual spin and the sum of the spins for the same system would be of a great interest because from this information one can determine the partitioning of angular momentum within the dinuclear complex. Unfortunately, if sequential fission occurs with a sufficiently high probability to make extraction of an individual spin experimentally feasible, then the relation between M_γ and the spin of the primary fragments is greatly obscured. This is due to the fact that the fissioning nucleus loses a substantial amount of its intrinsic spin to orbital angular momentum of the fission fragments. This difficulty can be substantially reduced by employing the sequential emission of light particles as the probe of the spin of one of the DI fragments.¹⁴⁻¹⁷ Light particle emission generally converts a much smaller fraction of the DI fragment's intrinsic spin into orbital angular momentum than does sequential fission and thus the difficulties of relating γ -ray multiplicity data to spin are

similarly reduced. Therefore, the determination of both the γ -ray multiplicity as well as the out-of-plane α -particle distributions for the same system is an attractive combination of techniques.

For the system 280 MeV $^{40}\text{Ar} + ^{58}\text{Ni}$, Babinet et al.,¹⁵ have shown that α -particle emission from the target recoil nucleus could be isolated by careful selection of the detection angles. Their results indicate that the intermediate complex is rotating rigidly. For systems of similar mass, 175 MeV $^{20}\text{Ne} + ^{\text{nat}}\text{Ag}$ (ref. 5) and 237 MeV $^{40}\text{Ar} + ^{89}\text{Yb}$ (ref. 9), M_γ data also indicate rigid rotation of the dinuclear system. For much heavier systems like $^{86}\text{Kr} + ^{197}\text{Au}$ and $^{86}\text{Kr} + ^{165}\text{Ho}$, the evidence for rigid rotation is indirect because of ℓ -wave fractionation effects.⁶

In this paper we report on an investigation of the transfer and partition of angular momentum in a deep-inelastic reaction for a system intermediate in mass between the light systems for which clear evidence for rigid rotation exists and the heavier systems where the evidence is masked by ℓ -wave fractionation. A brief account of this work has appeared previously.¹⁷ The choice of the 664 MeV $^{84}\text{Kr} + ^{\text{nat}}\text{Ag}$ system was motivated by several considerations. To insure an easy connection between the out-of-plane α -particle distributions and the original spin of the nucleus, it is important to have mainly first chance α -particle emission. However, in order for the experiment to be feasible, the α -particle multiplicity should not be too small. The Kr + Ag system satisfies these conditions. In addition, it has been shown^{9,18} that in this mass region M_γ can be rather directly related to the sum of the intrinsic spins.

To extract the spin of one of the deep-inelastic fragments, we must be able to measure the out-of-plane distribution of light particles which have been emitted from only one of the deep-inelastic fragments. A velocity

diagram of our experimental configuration is shown in Fig. 1. The circles indicate the locus of points for the most probable α -particle emission from fragments with atomic numbers 36 and 47. This figure indicates that if the out-of-plane data are acquired at an in-plane angle equal to or larger than the recoil direction, there should be little contamination from the projectile-like fragment. It should be noted that our experiment is designed to utilize the well-known and understood process of α -particle evaporation from excited nuclei to extract information concerning the spins of these nuclei. We are specifically trying to avoid detecting nonevaporative emissions, reports of which have appeared prolifically in the literature.^{3,19,20} We will show that the α -particles observed in this experiment are the result of evaporation from fully accelerated deep-inelastic fragments.

II. Experimental

In- and out-of-plane data were obtained in two separate experiments at the Lawrence Berkeley Laboratory SuperHILAC. The experimental setup is schematically depicted in Fig. 1b. Beams of ^{84}Kr impinged upon $^{\text{nat}}\text{Ag}$ targets with thicknesses of 0.97 mg/cm^2 and 0.59 mg/cm^2 for the in- and out-of-plane runs, respectively. The target was placed in a holder that could rotate about two perpendicular axes, thus allowing a choice of target angle and tilt to minimize the energy loss of alpha particles and heavy ions in the target. A gas ionization telescope (for the in-plane run) or a solid state telescope (out-of-plane run) was used to detect the projectile-like fragment. The ΔE -E telescope served to define the reaction plane and to identify the atomic number (Z) of the detected fragment. The Z-telescope was placed at $\phi_Z = 26^\circ$, slightly behind the grazing angle, with solid angles of 4.8 msr and 6.8 msr (corresponding to acceptance angles of $\pm 2.2^\circ$ and $\pm 2.7^\circ$) for the in- and out-of-plane experiments, respectively.

On the opposite side of the beam, an arc with both in- and out-of-plane arms was used to mount up to five light particle (LP) solid state $\Delta E-E$ telescopes (40 μm -5 mm). The arc was attached to a thin-walled domed lid, which, when placed on the scattering chamber, seated the foot of the arc into a cradle on an externally movable arm. The error in the angle of any LP telescope was estimated to be no more than 0.5° . The solid angles of the LP telescopes were measured with a ^{241}Am source of known activity and the relative efficiencies checked with a ^{212}Pb source. The solid angles of the LP telescopes agreed to within $\pm 3\%$ of the geometric solid angle. Absorbers ranging from 10.1 mg/cm^2 Ta to 1 mg/cm^2 Au were placed in front of the LP telescopes to reduce the rates of heavy ions, X-rays, and low energy electrons striking these counters. The detection threshold for α -particles was approximately 10 MeV, primarily due to the thickness of the first element of the telescope rather than to the absorbers.

An array consisting of eight (in-plane run) and seven (out-of-plane run) 7.6 x 7.6 cm NaI detectors was utilized to measure the γ -ray multiplicity (M_γ). These detectors were positioned above the reaction plane at an out-of-plane angle of 45° and at a distance of 23 cm from the target. This distance was sufficient to separate neutrons from γ rays by their time of flight.²¹ In the out-of-plane run, an eighth NaI with a reduced solid angle was used to obtain γ -ray energy data.

Double (Z,LP), triple, higher order (Z, LP, XY) coincidence events, as well as scaled down Z and LP singles events were recorded on magnetic tape in an event-by-event format. Light particle singles data were obtained every 5° from 20° to 105° . Coincidence data were obtained at 10 in-plane and 6 out-of-plane angles (with an in-plane projection approximately coinciding with the target recoil direction). A real-to-random rate of $\sim 40/1$

was obtained for the out-of-plane data, which was improved to $\sim 100/1$ for the in-plane data by running slightly lower beam currents. A summary of the angles, absorbers and solid angles for the coincidence data is provided in Table 1.

III. Data and Analysis

1) Lab System

Detailed inclusive studies²² of the energy, charge and angular distributions for the fragments produced in the Kr + Ag reaction have been reported previously for several bombarding energies. A very prominent deep-inelastic component has been observed with an associated broad charge distribution and a forward peaked angular distribution. In Fig. 2a the inclusive secondary charge distribution (after particle evaporation) measured at $\phi_{\text{lab}} = 26^\circ$ is shown. This charge distribution increases monotonically as the Z-value increases toward symmetry, as has been observed in previous inclusive studies²². The atomic numbers of the projectile-like fragment were identified up to $Z = 41$.

The fragment total kinetic energies (TKE) were calculated event-by-event from the measured kinetic energies assuming two body kinematics and were corrected for pulse-height-defect, absorber losses and particle evaporation effects. Part b of Fig. 2 shows the TKE spectrum integrated over the Z-values shown in part a. A strong DI component is observed that is well separated from the quasielastic component. Since we were interested in α -particle emission from fully relaxed collisions, only Z- α coincidence events which satisfied the gate shown in Fig. 2b were analyzed. The high-energy shoulder above the elastic peak is due to a small amount of a heavy target contaminant which adds a negligible contribution to the DI-region of the TKE spectra.

Representative singles α -particle energy spectra are shown in Fig. 3a for three lab angles. An increase in the complexity of the spectral shape is observed as the lab angle decreases from 90° to 30° . This is not unexpected. Since the measured evaporation residue cross section for this system is less than 50 mb^{23} , the only emission source that should significantly contribute at backward angles is the target-like recoil, while at forward angles both fragments, with a large variety of velocities, act as emission sources. Requiring a coincidence with a DI fragment simplifies the α -particle spectra as shown in Fig. 3b. These energy spectra, which are generated with the requirement of a coincidence with a fragment having $26 \leq Z \leq 40$ and a TKE in the DI region, are shown for the same angles as part a. At 90° the singles and coincidence spectra are similar. This confirms our expectation that at this backward angle the bulk of the α -particles are emitted from the target-like recoil. At 60° , the coincidence spectrum again shows only one component, whereas the singles spectrum shows an additional low-energy component. At the most forward angle the singles spectrum is quite complex, whereas the coincidence spectrum can be qualitatively interpreted in terms of a strong component from the target recoil and a weak one from the detected fragment. This latter component has a lower energy in the lab system because it results from the backward emission from a fast-moving source (see Fig. 1a).

The integrals of the α -particle energy spectra are shown in Fig. 4 as a function of lab angle for both the singles a) and coincidence b) data. The singles angular distribution shows a strong forward peaking. This anisotropy is primarily due to the multiplicity of forward moving emission sources. Setting the DI and Z- α coincidence requirements decreases the forward peaking. This is the result of the substantial reduction of strongly forward

peaked components, such as emission from the projectile-like fragment. To determine whether or not the main component in the coincidence spectra results from the statistical evaporation from the target-like DI product, the energy spectra must be examined in the rest frame of the emitter.

2) Rest frame

The velocity of the recoil fragment was calculated from the momentum of the projectile-like fragment by invoking momentum balance and utilizing masses calculated by assuming that the neutron to proton ratio is equilibrated. Thus, for a given mass asymmetry, the charge asymmetry is that which minimizes the sum of the liquid drop energies. Two dimensional plots of the calculated values of both the TKE and recoil angle vs. the atomic number of the detected fragment are shown in Fig. 5a and b, respectively. The cluster of intensity at large TKE values and recoil angles of $\sim 70^\circ$ with Z of 36 ± 1 is attributable to elastic and quasielastic events. The DI component (see Fig. 5a) shows a gradual increase in TKE as the system becomes more symmetric. For a deep-inelastic reaction the TKE is approximately the sum of the Coulomb energy and the orbital rotational energy of the dinuclear complex. The above TKE dependence results from the fact that the dominant Coulomb term reaches a maximum for the symmetric dinuclear system.

In Fig. 5b it is seen that for the DI component the recoil angle varies with mass asymmetry from approximately 10° for the lightest detected fragments to 50° for symmetric divisions. For the region $26 \leq Z \leq 40$, the cross-section-weighted average recoil angle is $\phi_L \sim 40^\circ$ with a FWHM of 16° . The evaporation correction amounts to 7° for $Z = 36^\circ$.

The in-plane angle associated with the out-of-plane detectors was $\phi_L = 41^\circ$, approximately coinciding with the average direction of the target-like recoil fragment. This in-plane angle was chosen after considering the problem of making the transformation from the lab system into the rest frame of the target-like recoil. In Fig. 6 contours of equal in- (ϕ_{RF}) and out-of-plane (θ_L) angles in the rest frame of the emitter are plotted as a function of the in- (ϕ_L) and out-of-plane (θ_L) lab angles. From this plot it can be seen that if one measures an out-of-plane distribution at a fixed in-plane angle of say, $\phi_L = 60^\circ$, then the out-of-plane distribution starts at an in-plane angle of about 90° from the recoil in the rest frame. However, when one reaches an out-of-plane lab angle of $\theta_L = 60^\circ$, corresponding to $\theta_{RF} \sim 60^\circ$, the in-plane angle in the recoil frame is $\phi_{RF} \sim 130^\circ$. The kinematics also indicates that at an in-plane lab angle of 60° , one cannot observe out-of-plane angles greater than 60° in the frame of the recoil. If the in-plane distribution of alpha particles has a dependence on ϕ_{RF} , then the out-of-plane distributions at fixed ϕ_L could be quite complicated due to the mixture of many ϕ_{RF} angles. On the other hand, if there is no dependence on ϕ_{RF} , then all out-of-plane distributions would be identical except that the maximum accessible out-of-plane angle in the rest frame (θ_{RF}) measurable at fixed ϕ_L decreases as ϕ_L increases. The considerations stated above led us to choose the target recoil direction as the in-plane angle at which to obtain the out-of-plane distributions.

If the strong component observed in the coincident lab energy spectra is the result of evaporation from the target-recoil nucleus, then the α -particle spectra in the recoil frame should have the same spectral shape. Several α -particle energy spectra in the recoil rest frame are shown in Fig. 7 for representative in- and out-of-plane angles. These spectra were obtained in

coincidence with projectile-like fragments ($26 \leq Z \leq 40$) having a TKE in the DI window. With the exception of the 30° data, these spectra are well described by an evaporation spectrum with a nuclear temperature, T , of approximately 2.9 MeV. In addition the location of the peak of the energy spectra is independent of angle in this rest frame. The small difference observed in the peak positions for the in- and out-of-plane spectra is within the uncertainty in the energy calibrations for the two experimental runs.

The two most forward angles (30° and 42°) contain a weak low-energy component, attributable to backward emission from the fast-moving projectile-like fragment. The only feature in these spectra that is not understood in terms of evaporation from excited nuclei is the excess of higher energy ($E_\alpha^{RF} \geq 15$ MeV) α -particles observed at the most forward angle (30°).

The uniformity of these spectra as a function of angle strongly suggests that these α -particles are emitted from the fully accelerated target-like fragment. This conclusion is also supported by the examination of the above data in the center of mass of the compound system (Fig. 8). A shift in the peak position to higher energies is observed as one moves to larger angles implying that the true moving source must be moving in some direction with a large ϕ_L . In fact, the magnitude of the shift in the peak seen in Fig. 8 can be readily understood if the rest frame is that of the target recoil.

Figures 7 and 8 indicate that the bulk of the emission is due to evaporation from the target-like fragment. This is in itself an interesting result apparently at variance with previous work^{24,25}, for a system that has similar²⁵ total mass and charge, suggesting that the bulk of light particle emission arises from the compound system prior to scission. At the present time, the reason for the difference between the results of the present study and those mentioned above is unclear.

The integrated in- and out-of-plane angular distributions expressed as differential multiplicities¹⁴ in the rest frame of the emitter, are shown in Fig. 9a and b. (The weak low-energy component from the projectile-like fragment, which is seen in the energy spectra of the most forward data, has been subtracted.) The in-plane data exhibit very little angular dependence for the eight most backward angles. This is consistent with isotropic in-plane emission from the target-like fragment. However, a substantial increase above the average of these backward angles (dashed line) is seen for the two most forward angles. This increase in yield is correlated with the high-energy α -particles seen in the energy spectra for these forward measurements. These α -particles have energies above 15 MeV in the rest frame of the recoil, corresponding to a lab energy of ~ 40 MeV.

In contrast to the in-plane angular distributions, the out-of-plane yield decreases smoothly with increasing out-of-plane angle, exhibiting an anisotropy of approximately 2. Integration of the differential multiplicity over ϕ_{RF} and θ_{RF} results in an average total α -particle multiplicity of 0.47 for the DI products having Z values between 26 and 40.

Since the anisotropy of the out-of-plane angular distributions of sequentially emitted particles should increase with the spin of the emitter, it is of interest to see how sensitive these distributions are to the γ -ray multiplicity. In Fig. 10a angular distributions for six Z-bins are shown. (Here the distributions are labeled by the charge of the emitting fragment.) In part b of this figure angular distributions are shown for the same Z bins but with the additional requirement that two or more γ rays be in coincidence with the α -particle and the DI fragment. In the mass region covered by this study, the γ -ray multiplicity is linearly related to the sum of the spins of the two fragments.^{9,18} Thus, requiring an increasing number of γ -rays to be

in coincidence with Z- α events should bias the fragment's spin distribution towards larger values and result in a greater focusing of the angular distribution into the reaction plane.[†] This effect is clearly seen when parts a and b of fig. 10 are compared. For rigid rotation of the dinuclear system, the individual fragment's spin changes strongly with the mass asymmetry of the exit channel. In Fig. 10a a gradual sharpening of the angular distributions as the charge of the emitter increases is evident, tentatively indicating that the fragment spin does increase with the mass asymmetry.

IV. Evaluation of the Fragment Spins

In order to extract fragment spins from the out-of-plane α -particle distributions, we have utilized the formalism of Moretto et al.,^{26,27} To facilitate a comparison with other work and to stress the importance of the various parameters, we have employed the formalism of ref. 27 at several different levels of sophistication, each of which will be described in this section.

Statistical mechanics predicts a Gaussian distribution for the projection (K) of the angular momentum on the heavy ion-evaporated particle separation axis. More specifically the decay width can be written as

$$\Gamma \propto \exp\left[\frac{-\hbar^2 I^2}{2I} \left(\frac{1}{J_{\perp}} - \frac{1}{J_c}\right) \exp\left(\frac{-K^2}{2K_0^2}\right)\right] \quad (1a)$$

where

$$K_0^2 = \frac{I}{\hbar^2} \left(\frac{1}{J_{\parallel}} - \frac{1}{J_{\perp}}\right)^{-1} \quad (1b)$$

The quantities \mathcal{J}_{\parallel} and \mathcal{J}_{\perp} are the moments of inertia parallel and perpendicular to the separation axis at the critical shape for alpha-particle decay, while \mathcal{J}_c is the moment of inertia for the compound system. The angular distribution is obtained by expressing the angle (α) between the total angular momentum I , and the separation axis with unit vector \hat{n} in terms of the polar angles ϕ' and θ' .

$$K = I \cos \alpha = \vec{I} \cdot \hat{n} = I_x \sin \theta' \cos \phi' + I_y \sin \theta' \sin \phi' + I_z \cos \theta'. \quad (2)$$

If the direction of the angular momentum is fixed, we may choose our coordinate system such that $I_x = I_y = 0$ and $I_z = I$. Under this condition of total alignment of the angular momentum, the angular distribution is given by

$$\omega^{(1)}(\theta') \propto \exp\left(\frac{-I^2 \cos^2 \theta'}{2K_0^2}\right) \propto \exp\left(\frac{I^2 \sin^2 \theta'}{2K_0^2}\right). \quad (3)$$

This relation can also be derived from the Ericson and Strutinski²⁸ formalism by integrating over the distributions of orbital angular momenta and energy of the emitted particles.²⁹ This expression has been employed in the analysis of previously reported deep-inelastic¹⁵ and compound nucleus data.³⁰

Since there is good evidence for rather large misalignments of the fragment spins in deep-inelastic reactions,³¹ this effect should be included in the angular distribution formalism. If the spin alignment of one fragment is described by Gaussian distributions in the Cartesian components of the angular momentum with variances σ_x^2 , σ_y^2 , and σ_z^2 , then the light particle decay width is given by^{32,27}

$$\Gamma(\theta', \phi') \propto \exp\left[\frac{-I^2 \hbar^2}{2I} \left(\frac{1}{\mathcal{J}_{\perp}} - \frac{1}{\mathcal{J}_c}\right)\right] \frac{1}{S(\theta', \phi')} \exp\left[\frac{-I^2 \cos^2(\theta')}{2S^2(\theta', \phi')}\right] \quad (4a)$$

with

$$S^2(\theta', \phi') = K_0^2 + \sigma_x^2 \cos^2 \phi' \sin^2 \theta' + \sigma_y^2 \sin^2 \phi' \sin^2 \theta' + \sigma_z^2 \cos^2 \theta' \quad (4b)$$

which gives a form similar to equation 3 for the angular distribution,

$$\omega^{(2)}(\theta', \phi') \propto \frac{1}{S(\theta', \phi')} \exp \left[\frac{-I^2 \cos^2 \theta'}{2S^2(\theta', \phi')} \right] \quad (5)$$

By fitting equation 5 to an out-of-plane distribution one can extract the root-mean-square spin of the primary spin distribution biased by the angular momentum dependence of α -particle emission. However, since it is reasonable to expect that the fragment spin distribution will reflect the entrance channel angular momentum distribution, one can take the formalism a step farther by folding in this distribution. If the fragment's spin distribution is taken to be of the form $2I$ and bound by I_{\min} and I_{\max} , then the angular distribution is given by

$$\omega(\theta', \phi') = \int_{I_{\min}}^{I_{\max}} 2I \frac{\Gamma_{\alpha}(\theta', \phi')}{\Gamma_T} dI \quad (6)$$

This expression depends upon the relative magnitude of the alpha and neutron total decay widths. These widths can be determined from experimental data or the ratio,

$$\frac{\Gamma_{\alpha}}{\Gamma_n} = \Delta e^{I^2 \beta} \quad (7a)$$

$$\text{where } \Delta = 2 \exp \left\{ -(BE_{\alpha} + CB_{\alpha} - BE_n)/T \right\} \text{ and} \quad (7b)$$

$$\beta = \frac{\pi}{2T} \left(\frac{1}{J_n} - \frac{1}{J_{\alpha}} \right) \quad (7c)$$

In the expression for Δ , BE_{α} and CB_{α} are the α -particle binding energy and Coulomb barrier for α -particle emission, while BE_n is the neutron binding energy. The parameter β accounts for the change in the relative α/n decay

widths as a function of angular momentum. This parameter depends upon the moment of inertia of the residual nucleus after neutron emission, \mathcal{J}_n , as well as \mathcal{J}_1 and the nuclear temperature (T). If the ratio Γ_α/Γ_n is small, then $\Gamma_T \sim \Gamma_n$ and the integral in equation 6 can be evaluated, with the analytical result,

$$\omega^{(3)}(\theta', \phi') \propto (e^{-I_{\min}^2 A} - e^{-I_{\max}^2 A}) / S(\theta', \phi') A \quad (8a)$$

$$\text{where } A = \frac{\cos^2 \theta'}{2S(\phi', \theta')} - \beta \quad (8b)$$

If Γ_α is not much smaller than Γ_n then the integral in equation 6 can be solved for $\Gamma_T = \Gamma_n + \Gamma_\alpha$ to yield the more complicated expression given below:

$$\omega^{(4)}(\theta', \phi') \propto \left(Q_{\min} e^{-I_{\min}^2 A} - Q_{\max} e^{-I_{\max}^2 A} \right) / S(\theta', \phi') \quad (9a)$$

where

$$Q_i = \left\{ \ln(e^{-\beta I_i^2} + \Delta) / 2\beta + \frac{I_i^2}{2} + \frac{1}{2A} + \frac{A}{\beta} \sum_{n=1}^{\infty} \frac{(-1)^n e^{-n I_i^2 \beta}}{2n(A-n\beta)} \right\} \quad (9b)$$

For comparison we have fit the data shown in fig. 9a to the four forms of the angular distribution described above. The calculation of the input parameters as well as the extracted spins are discussed in the next section.

V. Results and Discussion

The root-mean-square spin values for the heavy fragment, extracted as a function of exit channel charge asymmetry, are shown in table 2. The errors listed in this table represent only the statistical error. The columns correspond to different levels of sophistication in the formalism used to

extract the spins. The spins in columns a and b both result from fitting equation 3 to the out-of-plane distributions. These two sets of spins differ only in the method used to calculate K_0^2 . To generate the spins in the first column we took the critical shape for decay of the α -particle-residual nucleus system as two touching spheres. With this model the moments of inertia are given by

$$J_{\parallel} = J; J_{\perp} = J + \mu d^2 = J + \mu(r_0 M^{1/3} + R_{\alpha})^2. \quad (10)$$

Here, J is the moment of inertia of the residual nucleus and is equal to $2/5 MR^2$. We have used $R_{\alpha} = 2.53$ fm and $r_0 = 1.225$.

The trend of these extracted spins agrees with the predictions of rigid rotation of the deep-inelastic complex consisting of two touching spheroids. However, the magnitudes do not agree with the results from γ -ray multiplicity work. Both previous work⁶ and the present study obtained values for M_{γ} of less than 25 for all measured asymmetries. The total spins obtained from the M_{γ} data are shown in the last column of table 2. A comparison of these total spins (column g) with the individual spins (column a) extracted with equation 3 assuming a spherical critical shape for α -particle decay clearly indicates that the use of this configuration results in an overestimate of the fragment spin.

For the second column in table 2 the critical shape was taken as the equilibrium configuration of the rotating fragment- α complex in a spheroid-sphere model. This configuration is more extended along the separation axis than two touching spheres. This results in a reduced value of K_0^2 and in smaller spin values. This reduction in K_0^2 improves the agreement between the spin values extracted from the M_{γ} data and the α -particle distributions. This improved picture of the α -particle-residual nucleus system is used in the subsequent formulations of the angular distribution.

The spin misalignment is introduced by means of eq. 5. In employing this equation we have set $\sigma_x \approx \sigma_y \approx \sigma_z \equiv \sigma$. This approximate equality is suggested for near symmetric exit channels by our observation of a flat in-plane angular distribution as well as by theoretical work.³³ With this assumption S is no longer a function of angle, i.e. $S^2 = K_0^2 + \sigma^2$. The values of σ^2 were calculated using the model of Ref. 33. The inclusion of misalignment increases the spins by 2 to 3 \hbar (Table 2, compare columns b and c). The importance of the misalignment on the extracted spin value is related to the relative magnitude of σ^2 and K_0^2 . In our case $\sigma^2/K_0^2 \sim 1/4$; thus, including σ^2 changes S^2 by $\sim 25\%$ and therefore the fragment spin by only $\sim 10\%$. It is also clear from this ratio that in order to extract misalignments from light particle angular distributions, one needs to have very accurate values of K_0^2 as well as the fragment spins.

The spins contained in the next two columns of table 2 (d and e) are obtained from the spin-integrated forms of the angular distribution, respectively equations 8 and 9. The lower limit of integration, I_{\min} , was estimated from the lowest ℓ wave, ℓ_{\min} , leading to a nonevaporation residue event and then assuming rigid rotation of the intermediate complex. The value of ℓ_{\min} was calculated from the evaporation residue cross section²³ in conjunction with the sharp cutoff approximation.^{††} The parameter Δ was estimated from the total α -particle multiplicity considering the contribution to this multiplicity from second chance emissions. The spins from these integrated forms (columns d and e) agree within 5% of those obtained from the unintegrated form (column c).

The effect of gating on high M_Y events is seen in figure 11. Equation 8 was used to extract spins from the distributions with and without the requirement of at least two coincident γ rays. Gating on high M_Y events increases the average fragment spin by selecting out of the spin distribution the higher spin events. The average increase in spin per fragment is approximately $2 \hbar$.

Figure 11 also shows the rigid rotation prediction (curve) for two equally deformed spheroids. The predicted dramatic increase in fragment spin with increasing asymmetry is observed in the data (solid points) with the possible exception of the very asymmetric charge splits. In fact, rigid rotation of the intermediate complex is indicated by all of the methods of spin extraction described above (see Table 2).

The deformation of the DI complex is reflected also in the fragment kinetic energies. The fragment energies for two equally deformed spheroids is given by

$$E_L = \frac{M_H}{M_L + M_H} \left(\frac{Z_L Z_H}{d} F + \frac{\ell_{rel}^2}{2\mu d^2} \right) , \quad (11)$$

where the Coulomb correction factor (F), the distance between centers (d), and the relative angular momentum (ℓ_{rel}) are deformation dependent.

In Fig. 12a the experimental fragment kinetic energies, corrected for evaporation, are compared to calculations for several deformations. The calculations are for equally deformed spheroids separated by 1 fm. In this model, a ratio of axes (C/A) of about 2 is needed to reproduce the data,

indicating that the nuclei are substantially deformed. In Fig. 12b both individual spins and the sum of the fragment spins are presented along with rigid rotation predictions. These predictions are again for equally deformed spheroids with a ratio of axes of 2 separated by 1 fm. In the lower portion of this figure individual spins extracted from the α -particle distributions as described previously are shown (solid circles). Above this are plotted the sum of the spins of both fragments as determined by two independent methods. In the first method rigid rotation is invoked to determine the spin of the light fragment (I_L) from the value of I_H extracted from the out-of-plane α -particle distributions. Independently, we utilized the experimental M_γ data and the relation, $I_H + I_L = 2(M_\gamma - 6) + I_p$. The corrections (I_p) for the angular momentum removed by neutrons and α -particles were done following the prescription described in Ref. 34. These corrections average 28% and are therefore essential for a quantitative comparison between spins derived from M_γ and out-of-plane α -particle distributions. Both methods yield results that are relatively independent of mass asymmetry as has been observed in previous work.^{6,7,35} Since the calculations which assume rigid rotation and a constant Δ -window (see Fig. 12b) also exhibit only a weak mass dependence for the range of asymmetries populated in this system, it is difficult to draw any firm conclusions concerning rigid rotation from the change in the sum of the spins with mass asymmetry. It should be noted, however, that large deformations are again needed in order to obtain quantitative agreement with the summed spins, as is the case for the individual spins and the kinetic energies.

The sum of the spin values reported here agree with previous M_γ work on the same system.⁶ This previous work provided evidence that the failure of the γ -ray multiplicity to increase with increasing mass asymmetry, a trend

clearly seen in the very heavy systems $\text{Kr} + {}^{165}\text{Ho}$ and $\text{Kr} + {}^{197}\text{Au}$, was due to an ℓ -wave fractionation with exit channel mass asymmetry.^{6,36} The evidence presented in Refs. 6 and 36 for ℓ -wave fractionation in the nearly symmetric ${}^{84}\text{Kr} + {}^{\text{nat}}\text{Ag}$ system was much weaker. This is due to the fact that the experimentally accessible exit channels are near symmetric and thus even rigid rotation with a constant ℓ -window predicts a weak dependence of the sum of the spins on mass asymmetry. This is clearly seen in Fig. 2 of Ref. 6 as well as in the top portion of Fig. 12b. However, because an individual fragment spin is a much more sensitive probe, we see a strong rise in the individual fragment spin as a function of increasing asymmetry, which is the fingerprint of rigid rotation and a constant ℓ -window. This does not completely exclude the possibility of some ℓ -fractionation for the $\text{Kr} + {}^{\text{nat}}\text{Ag}$ system and there is some evidence for it at the largest mass transfers (see fig. 11 or 12b), where the measured spins fall below the rigid rotation calculation.

VI. Summary and conclusions

We have measured in- and out-of-plane α -particle distributions in coincidence with deep-inelastic projectile-like fragments for the reaction 664 MeV ${}^{84}\text{Kr} + {}^{\text{nat}}\text{Ag}$. At angles equal to or larger than the target recoil direction, the energy spectra are well described by evaporation from a fully accelerated target recoil nucleus. Furthermore, the in-plane distribution of alpha particles in the rest frame of the emitter is isotropic for angles greater than the recoil direction. In contrast, the out-of-plane distributions have an anisotropy of approximately 2 and show a dependence on the number of coincidence γ rays and the mass asymmetry of the deep-inelastic exit channel. From these out-of-plane distributions the spin of the emitting

nucleus was extracted. These spins, along with those extracted from a simultaneous γ -ray multiplicity measurement, have been used to study the transfer of orbital angular momentum into intrinsic spin and its partitioning within the dinuclear complex. These data provide unambiguous evidence for rigid rotation of the intermediate complex. Furthermore, large deformations are indicated by three sources: fragment kinetic energies, spins extracted from the out-of-plane α -particle distributions, and those deduced from γ -ray multiplicity data.

This work was supported by the Director, Office of Energy Research, Division of Nuclear Physics of the Office of High Energy and Nuclear Physics of the U.S. Department of Energy under Contract W-7405-ENG-48.

References

1. W.U. Schröder and J.R. Huizenga, *Ann. Rev. Nucl. Sci.* 27 465 (1977), and references therein.
2. L.G. Moretto and R. Schmitt, *J. Phys.* 37 (1976) C5-109 and references therein.
3. R. Albrecht, W. Dünneweber, G. Graw, H. Ho, S.G. Steadman, and J.P. Wurm, *Phys. Rev. Lett.* 34 1400 (1975).
4. M. Lefort and C. Ngô, *Rivista Del Nuovo Cimento* 2 1 (1979).
5. P. Glässel, R.S. Simon, R.M. Diamond, R.C. Jared, I.Y. Lee, L.G. Moretto, J.O. Newton, R. Schmitt, and F.S. Stephens, *Phys. Rev. Lett.* 38 331 (1977).
6. M.M. Aleonard, G.J. Wozniak, P. Glässel, M.A. Deleplanque, R.M. Diamond, L.G. Moretto, R.P. Schmitt, and F.S. Stephens, *Phys. Rev. Lett.* 40 622 (1978).
7. A. Olmi, H. Sann, D. Pelte, Y. Eyal, A. Gobbi, W. Kohl, U. Lynen, G. Rudolf, H. Stelzer, and R. Bock, *Phys. Rev. Lett.* 41 688 (1978).
8. C. Gerschel, M.A. Deleplanque, M. Ishihara, C. Ngô, N. Perrin, J. Peter, B. Tamain, L. Valentin, D. Paya, Y. Sugiyama, M. Berlinger, and F. Hanappe, *Nucl. Phys.* A317 473 (1979).
9. M.N. Namboodiri, J.B. Natowitz, P. Kasiraj, R. Eggers, L. Adler, P. Gonthier, C. Cerruti, and S. Simon, *Phys. Rev.* C20 982 (1979).
10. P. Dyer, R.J. Puigh, R. Vandenbosch, T.D. Thomas, M.S. Zisman, and L. Nunnolley, *Nucl. Phys.* A322, 205 (1979).
11. D.v. Harrach, P. Glässel, Y. Civelekoglu, R. Männer, and H.J. Specht, *Phys. Rev. Lett.* 42 1728 (1979).

12. M. Rajagopalan, L. Kowalski, D. Logan, M. Kaplan, J.M. Alexander, M.S. Zisman, and J.M. Miller, Phys. Rev. C19 54 (1979).
13. C. LeBrun, J.F. Lecolley, F. Lefebvres, M. L'Haridon, A. Osmont, J.P. Patry, and J.C. Steckmeyer, and R. Chechick, 6th Session d'etudes Biennale de Physique Nucleaire, Aussis, France, 2-6 Feb. 1981.
14. H.Ho, R. Albrecht, W. Dünweber, G. Graw, S.G. Steadman, J.P. Wurm, D. Disdier, V. Rauch and F. Scheibling, Z. Physik, A283 235 (1977).
15. R. Babinet, B. Cauvin, J. Girard, J.M. Alexander, T.H. Chiang, J. Galin, B. Gatty, D. Guerreau, and X. Tarrago, Z. Physik, A295 153 (1980).
16. W. Kühn, R. Albrecht, H. Damjantschitsch, H. Ho, R.M. Ronningen, J. Slemmer, J.P. Wurm, I. Rode, and F. Scheibling, Z. Physik, A298 95 (1980).
17. L.G. Sobotka, C.C. Hsu, G.J. Wozniak, G.U. Rattazzi, R.J. McDonald, A.J. Pacheco, and L.G. Moretto, Phys. Rev. Lett. (in press).
18. F.S. Stephens, Lawrence Berkeley Laboratory report LBL-10356, published in the Proceedings of the Varenna Conference, Varenna, Italy (1979).
19. J.W. Harris, T.M. Cormier, D.F. Geesaman, L.L.Lee, Jr., R.L. McGrath, and J.P. Wurm, Phys. Rev. Lett. 38 1460 (1977).
20. H. Utsunomiya, T. Nomura, T. Inamura, T. Sugitate, and T. Motobayashi, Nucl. Phys. A334 127 (1980).
21. L.W. Richardson, G.J. Wozniak, M.R. Maier, and L.G. Moretto, Nucl. Instr. and Meth. 173 485 (1980).
22. R.P. Schmitt, P. Russo, R. Babinet, R. Jared, and L.G. Moretto, Nucl. Phys. A279 141 (1976) and R.P. Schmitt, thesis, University of California at Berkeley (1978), Lawrence Berkeley Laboratory report LBL-7168 (1978).

23. H.C. Britt, B.H. Erkkila, P.D. Goldstone, R.H. Stokes, F. Plasil, R.L. Ferguson, and H.H. Gutbrod, Proceedings of the Symposium on Macroscopic Features of Heavy-Ion Collisions, Report ANL/PHY 76-2, 1976 (unpublished), p. 491.
24. D. Logan, M. Rajagopalan, M.S. Zisman, J.M. Alexander, M. Kaplan, and L. Kowalski, Phys. Rev. C22 104 (1980).
25. D. Logan, H. Delagrange, M.F. Rivet, M. Rajagopalan, J.M. Alexander, M. Kaplan, M.S. Zisman, and E. Duek, Phys. Rev. C 22 1080 (1980).
26. L.G. Moretto, Nucl. Phys. A247 211 (1975).
27. L.G. Moretto, S.K. Blau, and A.J. Pacheco, Lawrence Berkeley Laboratory report LBL-10805, Nucl. Phys. (in press).
28. T. Ericson and V. Strutinski, Nucl. Phys. 8 284 (1958).
29. T. Døssing, unpublished.
30. G.L. Catchen, M. Kaplan, J.M. Alexander and M.F. Rivet, Phys. Rev. C21 940 (1980).
31. G.J. Wozniak, R.J. McDonald, A.J. Pacheco, C.C. Hsu, D.J. Morrissey, L.G. Sobotka, L.G. Moretto, S. Shih, C. Schück, R.M. Diamond, H. Kluge and F.S. Stephens, Phys. Rev. Lett. 45 1081 (1980).
32. R.A. Broglia, G. Pollarolo, C.H. Dasso, and T. Døssing, Phys. Rev. Lett. 43 1649 (1979).
33. L.G. Moretto and R.P. Schmitt, Phys. Rev. C21 204 (1980).
34. S.K. Blau and L.G. Moretto, Lawrence Berkeley Laboratory report LBL-10926, Nucl. Phys. (in press).
35. P.R. Christensen, F. Folkmann, Ole Hansen, O. Nathan, N. Trautner, V. Videbaek, S.Y. Van Der Werf, H.C. Britt, R.P. Chestnut, H. Freiesleben and F. Pühlhofer, Nucl. Phys. A349 217 (1980).
36. R. Regimbart, A.N. Behkami, G.J. Wozniak, R.P. Schmitt, J.S. Sventek, and L.G. Moretto, Phys. Rev. Lett. 41 1355 (1978).

† Due to the angular distributions of stretched E2 and E1 γ radiation, to obtain the maximum bias of the spin distribution it is desirable to place γ -ray multiplicity detector array in the reaction plane. Unfortunately, experimental limitations did not allow us to get any closer to the reaction plane than 45° . However, at any angle, the requirements of a large number of coincident γ rays should bias the fragment's spin distribution towards large values.

†† It turns out that the extracted spin values are quite insensitive to I_{\min} . The spins extracted using the procedure to calculate I_{\min} described in the text and those extracted with $I_{\min} = 0$ are equal within statistical error.

Figure Captions

- Fig. 1. a) Velocity diagram for the reaction system. Circles indicate the most probable velocity for α -particle emission. The in-plane projection of the out-of-plane angles is indicated. The dashed arc indicates the detection threshold for the α -particle detectors.
b) Schematic view of the experimental setup. This figure depicts the Z-telescope, with its in-plane angle ϕ_Z ; light particle telescopes with in- and out-of-plane lab angles ϕ_L and θ_L respectively; and the array of NaI detectors with an out-of-plane angle of 45° .
- Fig. 2. a) Singles charge distribution in the lab system for projectile-like fragments at $\phi_Z = 26^\circ$.
b) Singles total kinetic energy spectrum in the lab system integrated over the Z-values shown in part a. Also shown is the deep-inelastic gate (DI).
- Fig. 3. a) Singles alpha-particle energy spectra in the lab system for three representative in-plane angles, see text.
b) Coincidence alpha-particle energy spectra in the lab system for the same angles as part a, see text.
- Fig. 4. a) Singles α -particle angular distribution in the lab system.
b) Coincidence in-plane α -particle angular distribution in the lab system.
- Fig. 5. a) Intensity plot of the lab total kinetic energy vs. charge of the projectile-like fragment for Z- α coincidence events.
b) Intensity plot of the calculated lab recoil angle of the undetected fragment vs. charge of the projectile-like fragment.

- Fig. 6. The correlation between the in- and out-of-plane angles for the detection of a light particle in the lab system (ϕ_L, θ_L) and the angles in the rest frame of the moving source (ϕ_{RF}, θ_{RF}) is shown. The in-plane lab angle is measured from the recoil angle rather than the beam direction. In this figure the velocity of the moving source, the target-like fragment, is 1.44 cm/ns. This was calculated from the kinetic energy of the projectile-like fragment utilizing two body kinematics. The velocity of the α -particle in the emitter's frame is 2.55 cm/ns, calculated from the expected most probable emission energy.
- Fig. 7. Coincidence alpha-particle energy spectra in the rest frame of the target recoil. Both in- and out-of-plane angles are shown.
- Fig. 8. Alpha-particle energy spectra in the center-of-mass of the overall system for three in-plane angles. These angles correspond to center-of-mass angles of 49° , 86° and 118°
- Fig. 9. Alpha-particle angular distributions in the rest frame of the target-like fragment in terms of the differential multiplicity. For this figure the charge of the projectile-like fragment satisfied the condition $26 \leq Z \leq 40$. The small contribution from the projectile-like fragment emission which is observed at forward angles (see Fig. 7) has been subtracted.
- a) In-plane distribution. The angle $\phi_{RF} = 0^\circ$ corresponds to the recoil lab direction. The dashed line is an average of the eight points for angles larger than the recoil direction.
- b) Out-of-plane distribution. The solid line is a fit to the data.

Fig. 10. Alpha-particle angular distributions as a function of out-of-plane angle for several Z-bins. Each bin is 3 Z units wide and is labeled by the median Z value. The distributions without any coincidence γ -ray requirement a) are expressed in units of differential multiplicity, whereas the distributions with two or more coincident γ rays b) are normalized to those in a) at 90° for the same Z bin. The solid lines are fits to the data (see Sect. IV).

Fig. 11. Spins extracted from the out-of-plane α -particle distributions with (open circles) and without (solid circles) the requirement of at least two coincident γ rays. Error bars are shown when they exceed the size of the symbol and indicate only the statistical error. The rigid rotation prediction for deformed spheroids with a ratio of axis of 2 and a separation of 1 fm is shown by the solid line.

Fig. 12. a) Center-of-mass energies as a function of the charge of the light fragment. The width of the symbols indicate the uncertainty in the primary charge (before evaporation). The curves are calculations for two equally deformed spheroids separated by 1 fm and are labeled by the ratio of axes. b) Plotted are: the spin of the heavy fragment extracted from the α -particle distributions (solid circles), the sum of spins calculated from α -particle data (squares), and M_γ data (open circles). The sizes of the solid symbols indicate the statistical error only.

Table 1

$\text{nat}_{\text{Ag}} + {}^{84}\text{Kr}$ (664 MeV)

In-plane			Out-of-plane		
Angle ϕ_L/θ_L (deg)	Absorber material (mg/cm^2)	Solid angle (msr)	Angle ϕ_L/θ_L (deg)	Absorber material (mg/cm^2)	Solid angle (msr)
30.0/0.0	Ta 8.5	7.0	41.0/ 4.1	Ta 10.1	13.4
35.0/0.0	Ta 8.5	7.0	41.0/14.1	Ta 10.1	13.4
45.0/0.0	Ta 8.5	6.9	41.0/29.1	Ta 10.1	13.4
50.0/0.0	Ta 8.5	6.9	41.0/39.1	Ta 10.1	13.4
60.0/0.0	Ta 8.5	6.9	41.0/54.1	Ta 10.1	13.4
65.0/0.0	Ta 8.5	6.9	41.0/64.1	Ta 10.1	13.4
75.0/0.0	Au 4.6	6.7			
80.0/0.0	Au 4.6	6.7			
90.0/0.0	Au 1.0	6.6			
95.0/0.0	Au 1.0	6.6			

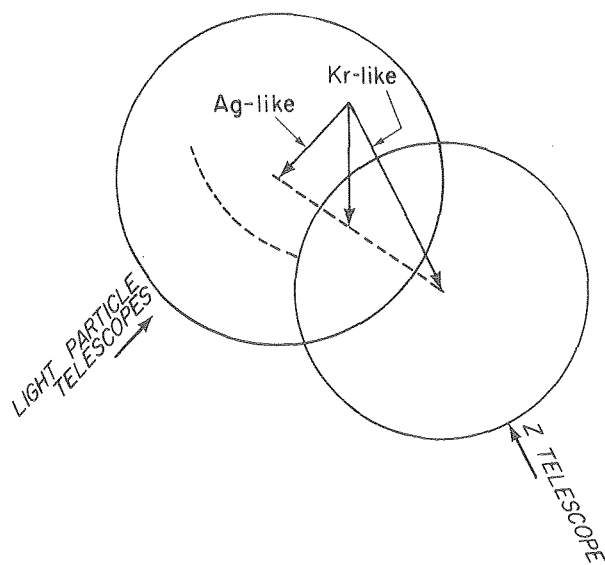
Table 2

Z_L	Z_H	$I_H(\hbar)$					$I_L + I_H (\hbar)$	
		a ω (1)	b ω (1)	c ω (2)	d ω (3)	e ω (4)	f ω (4)	g M_γ
~26	~57	39.8±0.9	27.3±0.6	29.6±0.7	28.4±0.3	29.2±0.2	36.8±0.3	38.7±2.0
~29	~54	38.0±0.6	26.5±0.4	28.9±0.5	27.7±0.2	28.5±0.3	38.2±0.5	39.9±2.0
~32	~51	33.7±0.6	24.1±0.4	26.6±0.4	25.4±0.2	26.2±0.2	37.7±0.4	40.8±2.0
~35	~48	30.3±0.5	22.1±0.4	24.6±0.4	23.6±0.2	24.3±0.2	38.0±0.4	39.2±2.0
~38	~45	26.3±0.5	19.4±0.4	22.0±0.4	21.0±0.2	21.5±0.2	37.8±0.4	35.4±2.0
~41	~42	21.4±0.7	16.2±0.5	18.6±0.6	17.9±0.2	18.3±0.2	36.1±0.4	36.7±2.0

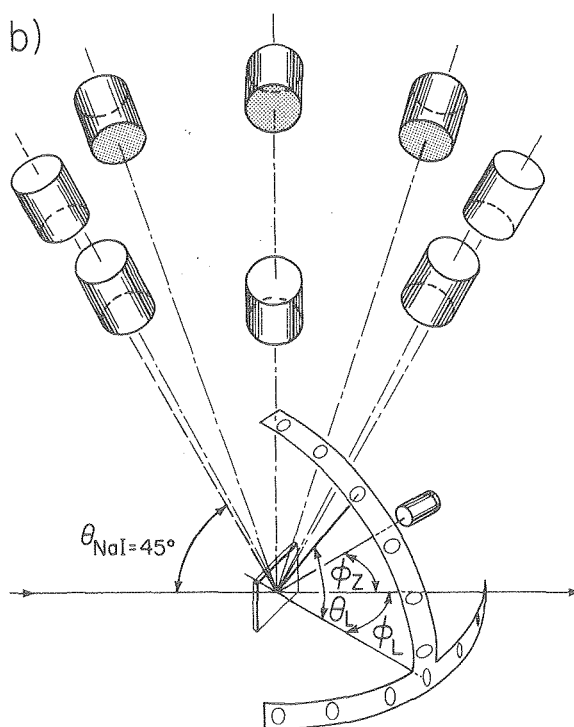
- a. Spherical K_0^2
- b. Equilibrium K_0^2
- c. Equilibrium K_0^2 , misalignment
- d. Equilibrium K_0^2 , misalignment, integration over spin distribution
with $\Gamma_T = \Gamma_n$
- e. Same as d, but with $\Gamma_T = \Gamma_n + \Gamma_\alpha$
- f. Calculated from column e assuming rigid rotation
- g. Calculated from experimental gamma multiplicities

a)

${}^{\text{nat}}\text{Ag} + {}^{84}\text{Kr}$ (664 MeV)



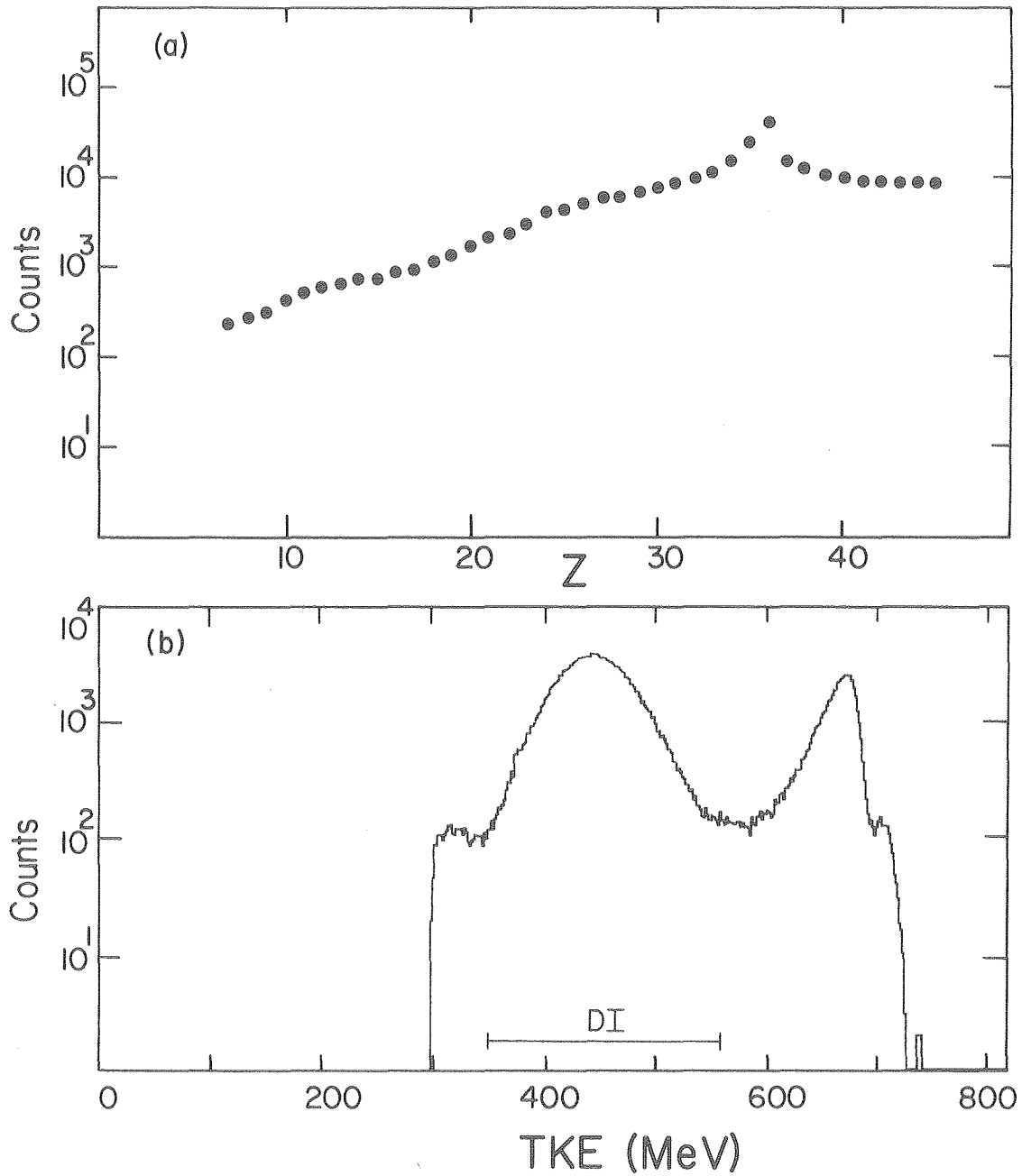
b)



XBL 8010-2227

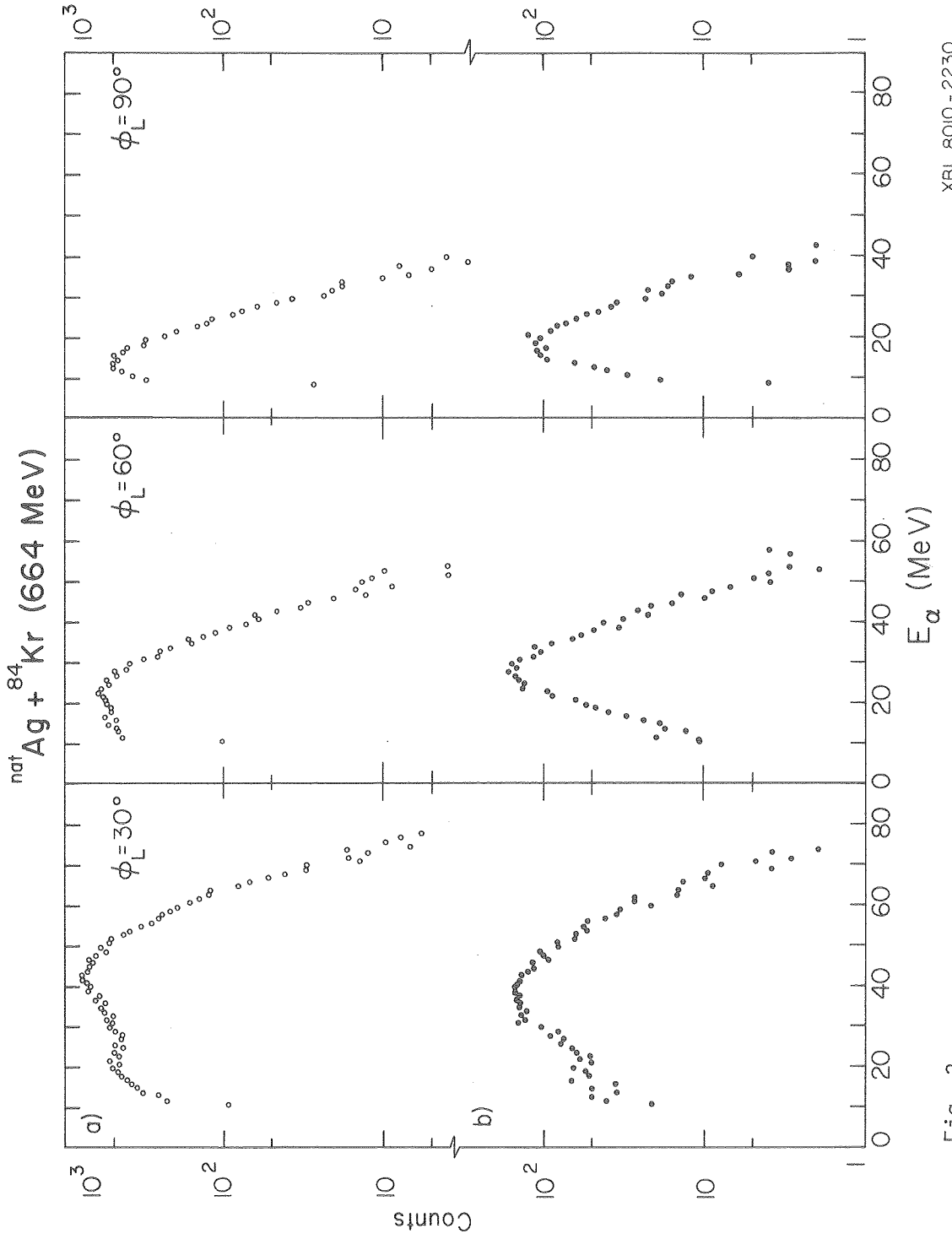
Fig. 1

$^{nat}\text{Ag} + ^{84}\text{Kr}$ (664 MeV)



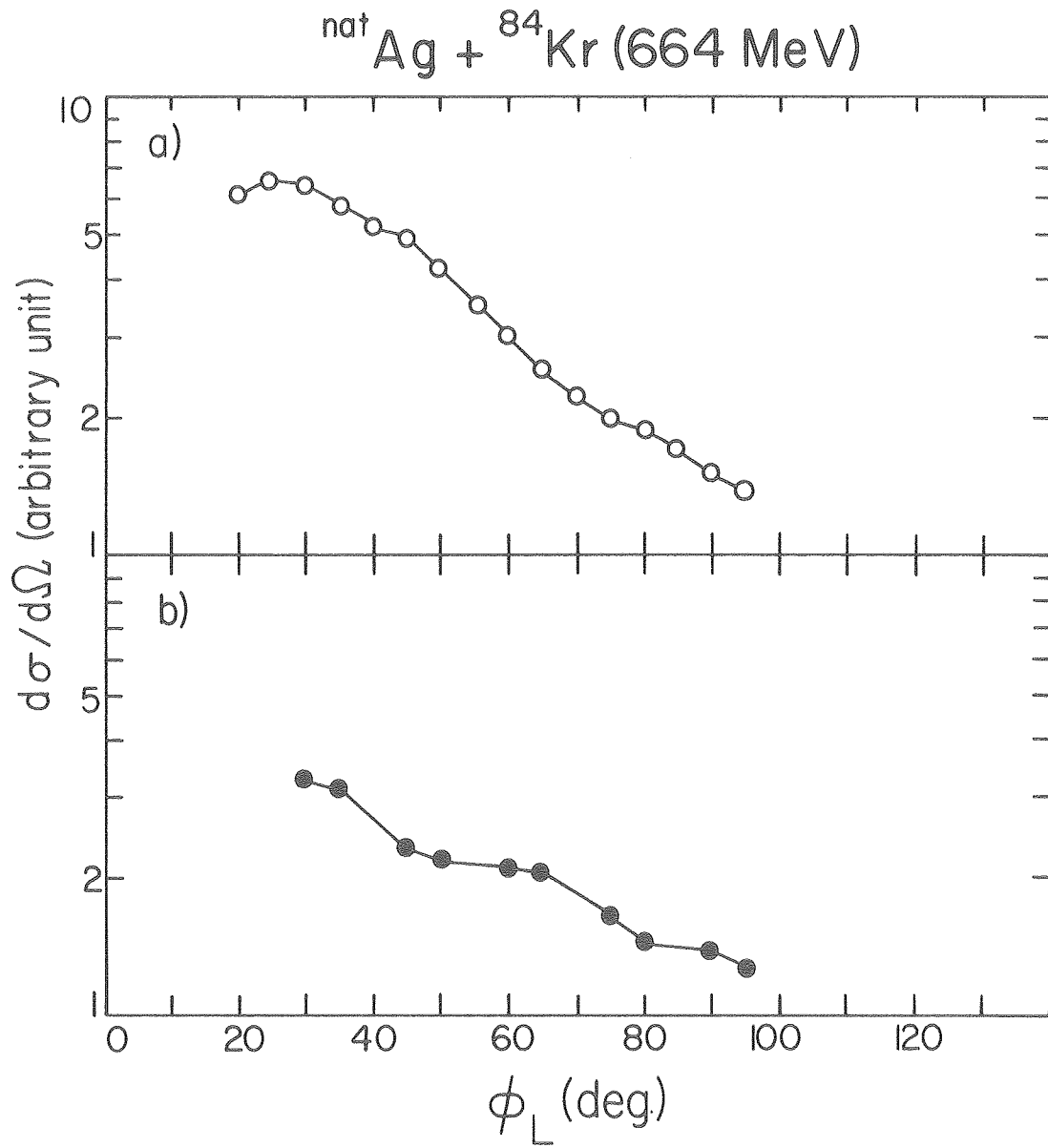
XBL 8010-2229

Fig. 2



XBL 8010 - 2230

Fig. 3



XBL 8010 - 2231

Fig. 4

$^{nat}\text{Ag} + ^{84}\text{Kr} (664 \text{ MeV})$

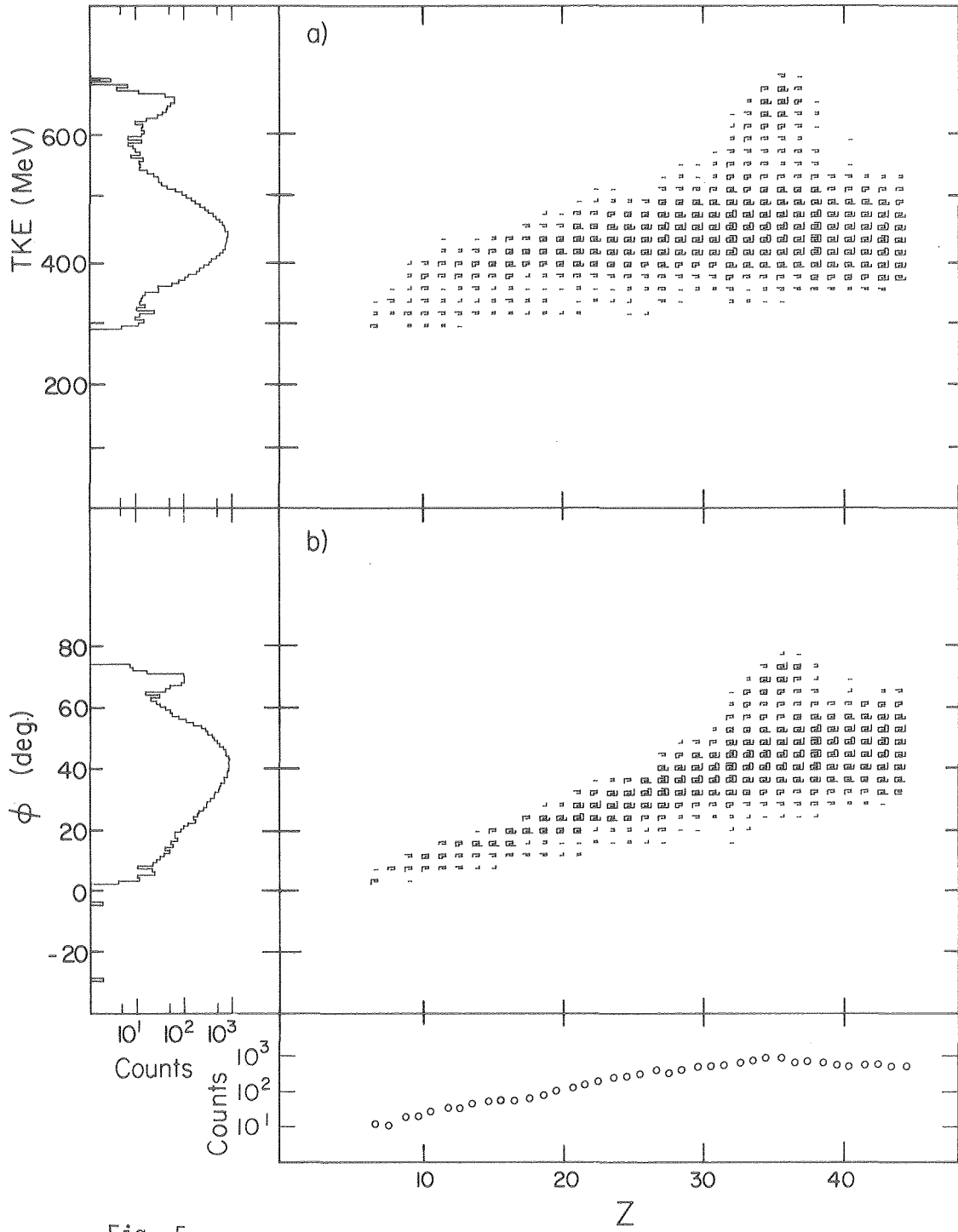


Fig. 5

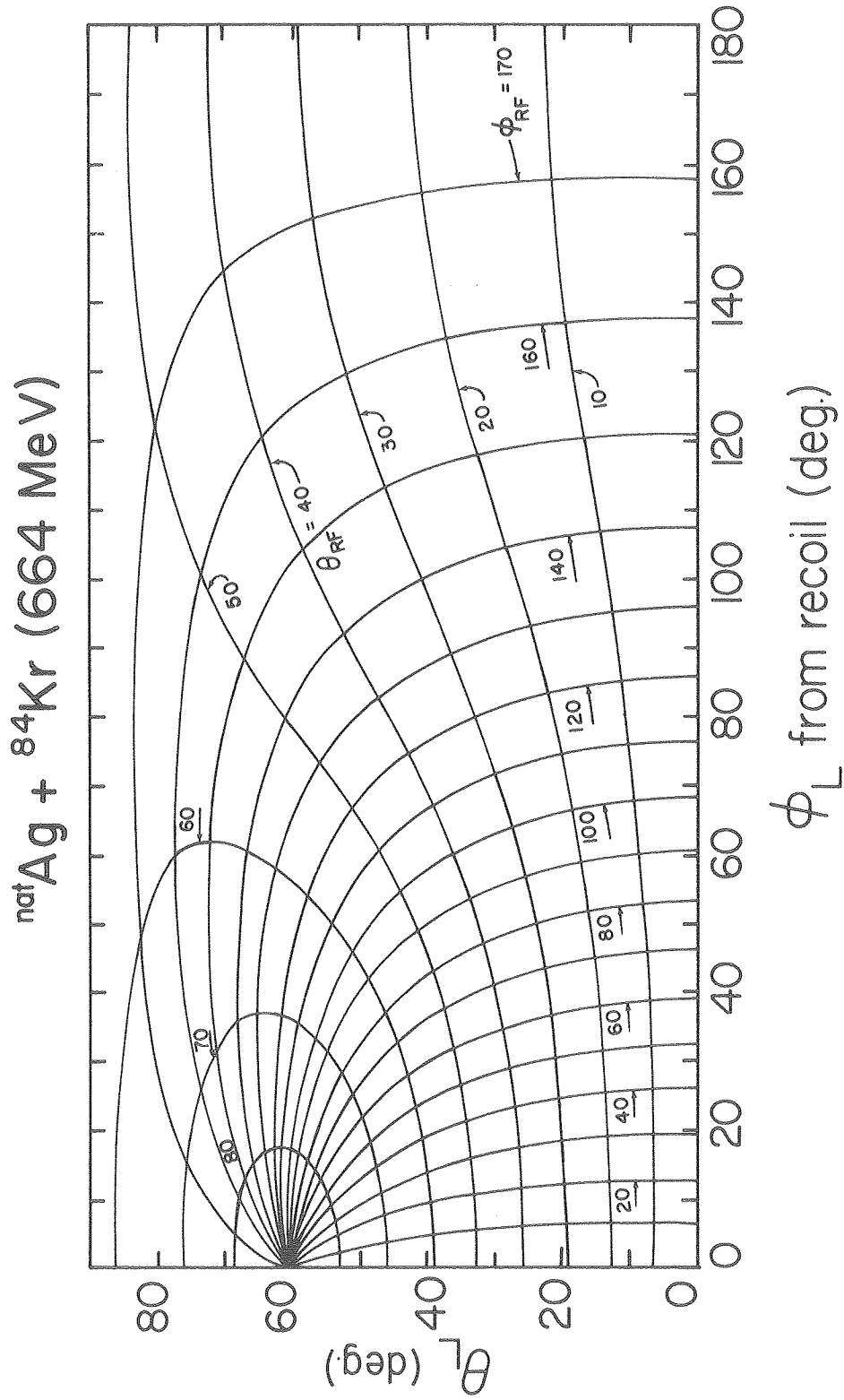
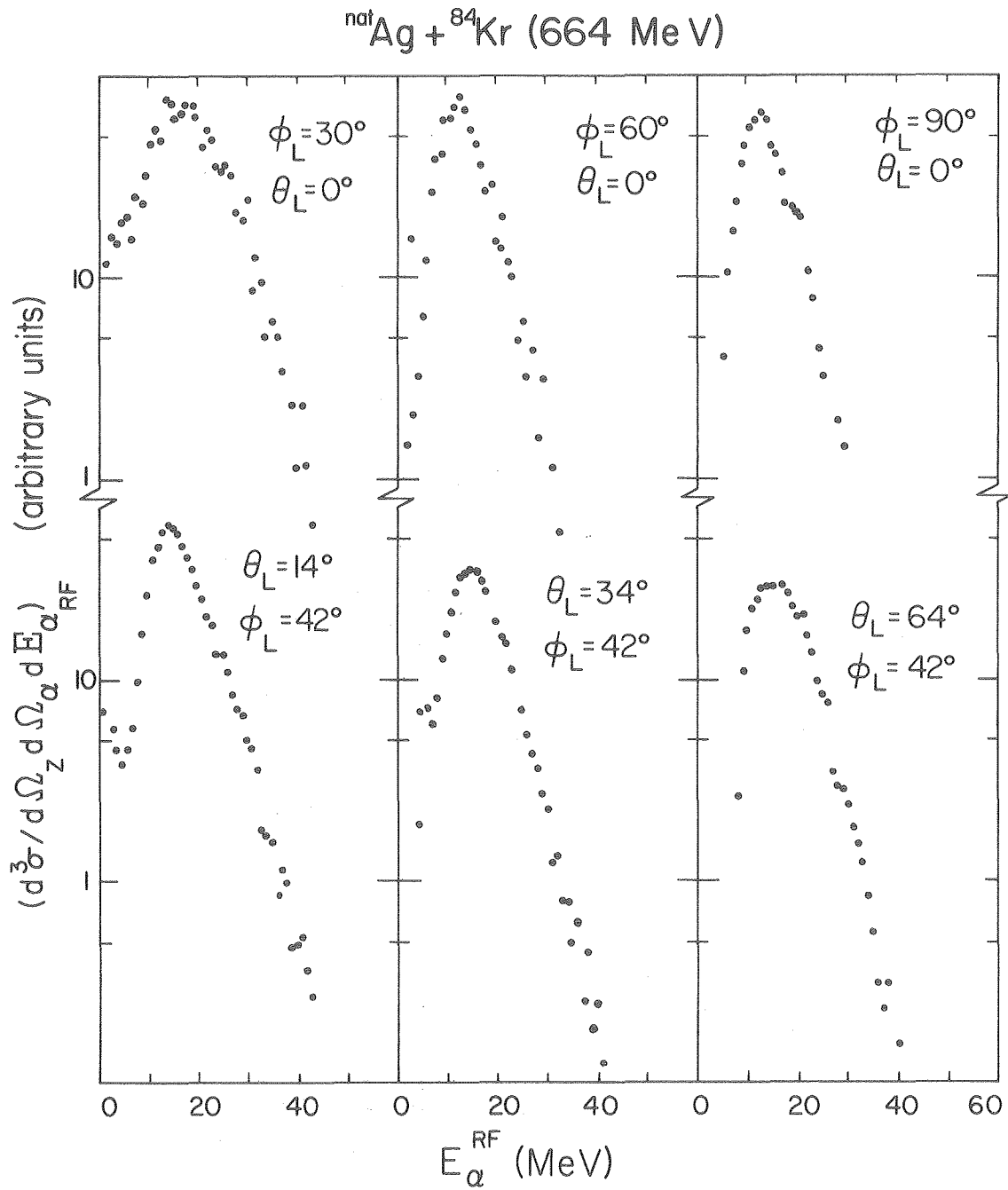


Fig. 6

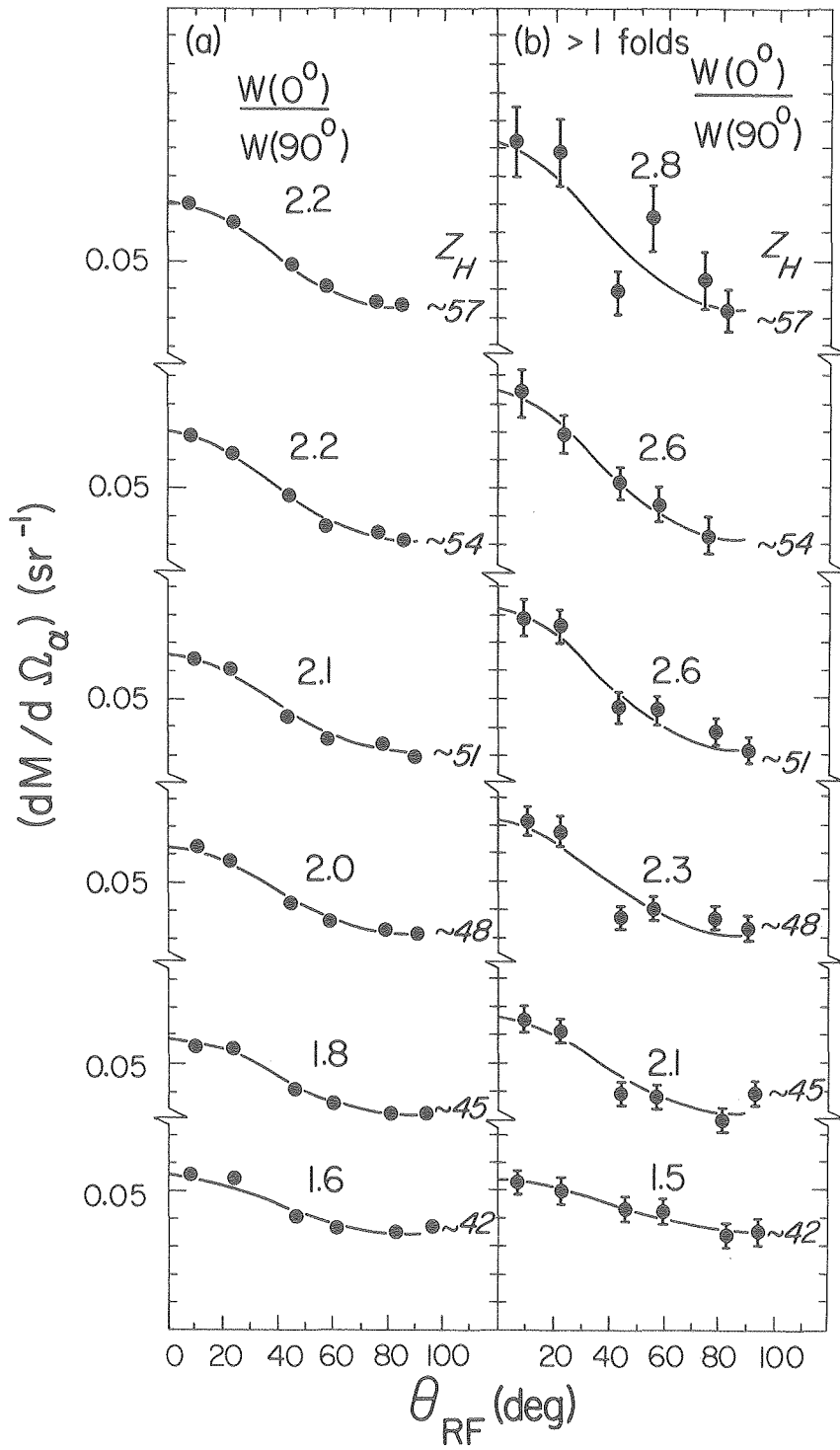
XBL 8010 - 2236



XBL 8010-2235

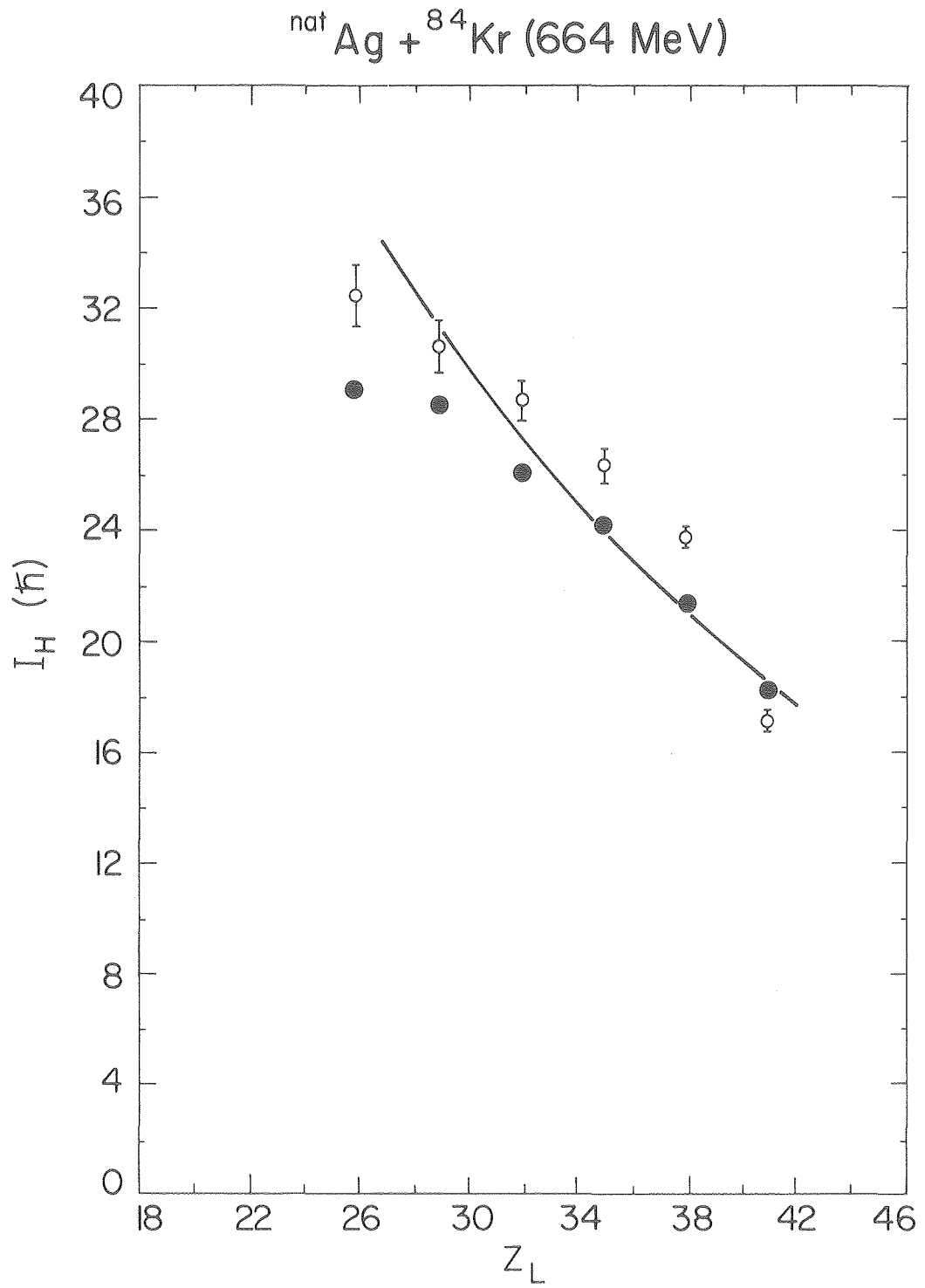
Fig. 7

nat Ag + ⁸⁴Kr (664 MeV)



XBL 811-93

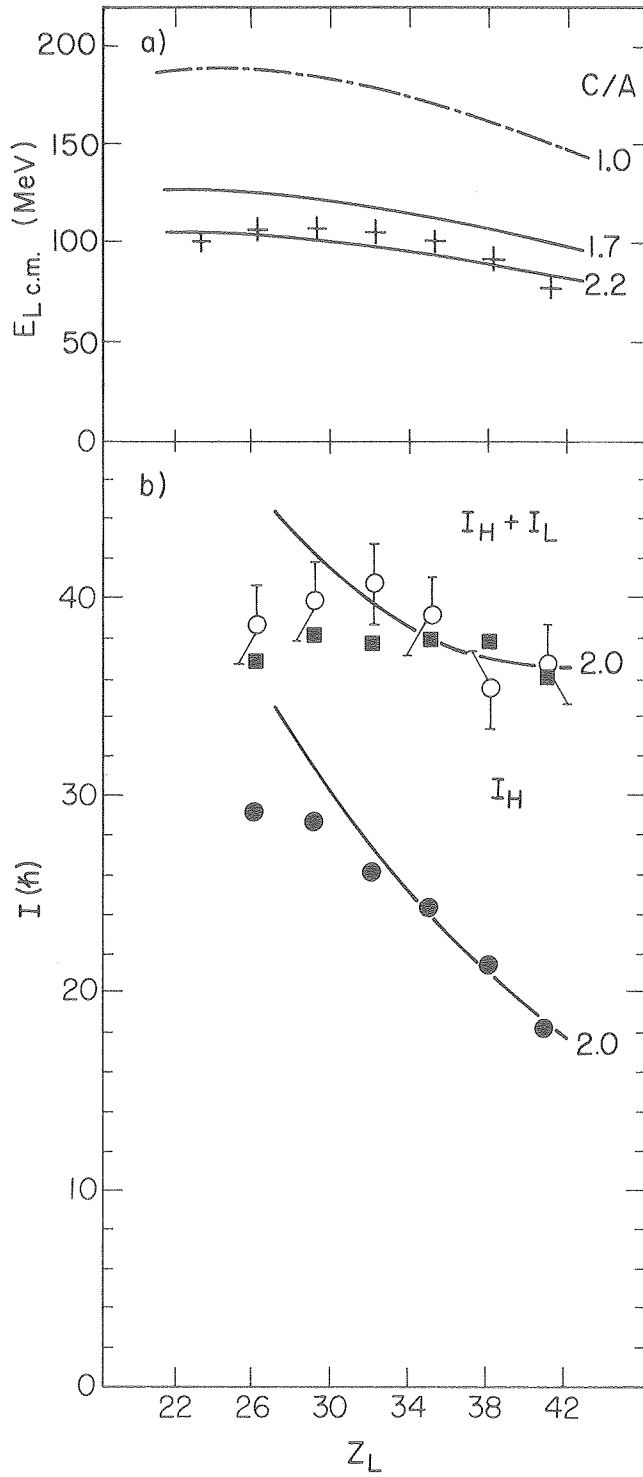
Fig. 10



XBL 8010 - 2228

Fig. 11

$natAg + {}^{84}Kr (664 MeV)$



XBL 807-3458 A

Fig. 12